Interplay of Turbulence and Proton-Microinstability Growth in Space Plasmas

Riddhi Bandyopadhyay, Ramiz A. Qudsi, William H. Matthaeus, Tulasi N. Parashar, and Bennett A. Maruca Department of Physics and Astronomy, University of Delaware, Newark, DE 19716, USA and Bartol Research Institute, Newark, DE 19716, USA

S. Peter Gary and Vadim Roytershteyn Space Science Institute, Boulder, Colorado 80301, USA

Alexandros Chasapis

Laboratory for Atmospheric and Space Physics, University of Colorado Boulder, Boulder, Colorado, USA

Barbara L. Giles and Daniel J. Gershman NASA Goddard Space Flight Center, Greenbelt, Maryland 20771, USA

Craig J. Pollock

Denali Scientific, Fairbanks, Alaska 99709, USA

Christopher T. Russell and Robert J. Strangeway University of California, Los Angeles, California 90095-1567, USA

Roy B. Torbert

University of New Hampshire, Durham, New Hampshire 03824, USA

Thomas E. Moore

NASA Goddard Space Flight Center, Greenbelt, Maryland, USA

James L. Burch

Southwest Research Institute, San Antonio, Texas 78238-5166, USA (Dated: February 21, 2020)

Both kinetic instabilities and strong turbulence have potential to impact the behavior of space plasmas. To assess effects of these two processes we compare results from a 3 dimensional particle-incell (PIC) simulation of collisionless plasma turbulence against observations by the MMS spacecraft in the terrestrial magnetosheath and by the Wind spacecraft in the solar wind. The simulation develops coherent structures and anisotropic ion velocity distributions that can drive micro-instabilities. Temperature-anisotropy driven instability growth rates are compared with inverse nonlinear turbulence time scales. Large growth rates occur near coherent structures; nevertheless linear growth rates are, on average, substantially less than the corresponding nonlinear rates. This result casts some doubt on the usual basis for employing linear instability theory, and raises questions as to why the linear theory appears to work in limiting plasma excursions in anisotropy and plasma beta.

The interplanetary plasma typically exhibits weak collisionality and strong turbulence [1, 2]. Similar conditions exist in many astrophysical systems. In such high-temperature, low-density magnetized plasmas, Coulomb collisions between particles are rare, which allows the velocity distribution fuction (VDF) of a given particle species to persist in a state far from local thermodynamic equilibrium. Consequently the VDFs are generally non-Maxwellian, and the distortions of the VDFs are manifested through substantial anisotropy in the pressure (or equivalently, temperature) tensor. Approximating the VDF as a bi-Maxwellian, the anisotropy in particle species j can be quantified as

$$R_{\rm j} = \frac{T_{\perp}^{\rm j}}{T_{\parallel}^{\rm j}}.\tag{1}$$

Here, $T_{\perp}^{\rm j}$ and $T_{\parallel}^{\rm j}$ are respectively the temperature of species j parallel and perpendicular to the local magnetic field (**B**).

Although deviations from equilibrium are observed in all charged plasma species [3–5], here we focus on protons. The extreme values of proton-temperature anisotropy in the solar wind exhibit a strong dependence on the parallel-proton beta [6–8]

$$\beta_{\parallel p} = \frac{n_{\rm p} k_{\rm B} T_{\parallel}^{\rm p}}{B_0^2 / (2 \mu_0)} , \qquad (2)$$

where, $n_{\rm p}$ is the proton number density, $k_{\rm B}$ is the Boltzmann constant, and μ_0 is the permeability of vacuum. For progressively larger $\beta_{\parallel p}$ values, the range of observed temperature-anisotropy values narrows in the solar wind [7] and the terrestrial magnetosheath [9].

Kinetic microinstabilities [10] offer an appealing theoretical explanation for the observed correlation between temperature anisotropy and plasma beta. Linearization of the Vlasov-Maxwell system about an assumed anisotropic equilibrium predicts that for extreme values of $R_{\rm p}$ and $\beta_{\parallel \rm p}$, the distribution function becomes unstable, triggering the growth of waves. It is typically assumed that upon reaching finite amplitude, these fluctuations drive the plasma toward (temperature) isotropy. The initial growth rate of the unstable waves is derivable via linear theory from the values of $\beta_{\parallel \rm p}$ and $R_{\rm p}$.

An important question is whether the unstable waves produced in this way are merely a passive "side effect", or if they actively modify the dynamics. Some authors adopt the interpretation that the ion-driven microinstabilities may "feed" strong fluctuations [11] in regions of instability, materially impacting the plasma dynamics. A different point of view is that turbulence-cascade generated localized inhomogeneities, i.e, coherent structures such as current sheets [12, 13], drive the temperature-anisotropies to extreme values, setting the stage for linear instabilities that might occur in regions of strong nonlinear effects.

The dissipation of turbulent fluctuations in weaklycollisional space plasmas involves the transfer of fluctuation energy from field and flow energies to thermal energies. The processes that contribute to this dissipation generally fall into one of two categories: strongly nonlinear intermittent processes, and quasilinear processes. Here, we use the term "nonlinear" to denote the former category which includes the cascade of turbulent energy from longer to shorter wavelengths where weak collisions and collisionless wave-particle interactions heat and isotropize the plasma species, and "linear" or "quasilinear" to denote the latter category whereby plasma anisotropies lead to the growth of shortwavelength plasma microinstabilities which also scatter, heat, and isotropize the plasma species. Within the limited scope of hybrid simulations, turbulence and microinstabilities have been shown to coexist [14-16].

Indeed, strong fluctuations are found near the same extreme regions of the $\beta_{\parallel p}$, R_p -plane where the instability growth rates are large, causing the plasma to remain (marginally) unstable to temperature-anisotropy instabilities [11, 17, 18]. Similarly, computations of sheardriven turbulence [19] have shown that local instabilities can sporadically arise due to kinetic effects that are inevitably found near current sheets and vortices [20, 21]. From these studies, it is evident that regions contributing to strong intermittency are also regions of strong kinetic activity, and furthermore these are often juxtaposed. It remains unclear which type of process - linear or nonlinear- dominates on average and determines the dynamics of large-scale phenomena. One may study this relationship by comparing the relative time scales of nonlinear and linear dynamical processes [22, 23]. There

is some subtlety in this comparison when the medium is inhomogeneous, in that intermittency enters into this comparison in a significant way, while the standard instability calculation that we employ assumes extended plane wave solutions.

Recent studies of turbulence-driven cascade and temperature-anisotropy driven microinstability [16, 22, 23] find that the majority of solar-wind intervals, in an idealized situation, would support the proton-driven microinstabilities. However, the associated growth rates are rarely faster than all the other relevant time scales. Quantitatively, the non-linear time scales, estimated from the spectral amplitude near the ion-inertial scale, are faster than the growth rates for most of the analyzed samples. This comparison suggests that the turbulent cascade quickly destroys the ideal situation for harboring micro-instabilities which would, otherwise, grow to macroscopic values as unstable modes.

As suggested above, the important physics of intermittency [24] motivates modification of results obtained from globally based estimates such as *average* non-linear time or *average* spectral amplitude near a given scale. Intermittent structures occupy a small fraction of the volume, but are likely responsible for a large fraction of the plasma heating and particle energization [25]. Keeping this in mind, we propose that, instead of comparing timescales based on average fluctuation amplitude with growth rates, it is reasonable to compare the two based on the corresponding local values of plasma and turbulence properties.

To address the above issues, here we carry out a local analysis of both the instability growth rates and the nonlinear time scales. We analyze three datasets:

- 1. A three-dimensional, kinetic, particle-in-cell (PIC) simulation,
- 2. In situ observations of Earth's magnetosheath by the MMS spacecraft, and
- 3. In situ observation of the interplanetary solar wind by the *Wind* spacecraft.

For all three cases we will show that both instability growth rates and non-linear rates are intermittent with enhanced values near coherent structures, and that, pointwise, the nonlinear processes are faster than the instabilities for a majority of cases.

Linear Vlasov Theory– Solving the dispersion relation for the linearized Vlasov and Maxwell's equations in a homogeneous plasma, one obtains the angular frequencies, ω , associated with a given wavevector \mathbf{k} . The imaginary component of ω is the growth or decay rate of the \mathbf{k} mode. The dominant growth rate of a particular instability, expected in linear theory to trigger macroscopic effects, is:

$$\gamma_{\max} \equiv \max_{\mathbf{k}} \Im(\omega) , \qquad (3)$$

where the maximum operation is taken over all wave-vectors \mathbf{k} associated with that instability. The plasma is considered unstable to a given instability if $\gamma_{\text{max}} > 0$.

To calculate these growth rates, the technique and software of [26] and [9] are employed. For each pair of $(\beta_{\parallel p}, R_p)$ -values, the value of γ_{\max} is determined for each of the four instabilities by computing the maximum value of $\Im(\omega)$ over a range of **k**-values. For every point with $\gamma_{\max} > 0$, we select the maximum growth rate from the 4 types of instabilities, associated with proton-temperature anisotropy:

$$\gamma = \max\{\gamma_{\max}^{\text{cyclotron}}, \gamma_{\max}^{\text{mirror}}, \gamma_{\max}^{\parallel-\text{firehose}}, \gamma_{\max}^{\nparallel-\text{firehose}}\}. \ (4)$$

Values of γ less than $10^{-5} \Omega_p$ are taken to be 0 (i.e., effectively stable). Note that in strong turbulence the plasma parameters vary significantly in space, so a separate calculation of γ is required at each point \mathbf{r} .

Nonlinear Timescales— The local nonlinear timescale, at a position \mathbf{r} , for a lengthscale ℓ can be estimated as

$$\tau_{\rm nl}(\mathbf{r}) \sim \ell/\delta b_{\ell},$$
 (5)

where the longitudinal magnetic field increment is

$$\delta b_{\ell} = \left| \hat{\boldsymbol{\ell}} \cdot \left[\mathbf{b}(\mathbf{r} + \boldsymbol{\ell}) - \mathbf{b}(\mathbf{r}) \right] \right|,$$
 (6)

and **b** is the *total* magnetic field expressed in Alfvén speed units. The vector lag ℓ has a magnitude ℓ and direction $\hat{\ell}$. The timescale $\tau_{\rm nl}({\bf r})$ is a strongly varying function of position, and may take on large values near coherent structures. Accordingly, we compare the local values of γ and $\tau_{\rm nl}$.

For comparison with instability growth rates, it is convenient to compute an equivalent frequency from the nonlinear timescales as $\omega_{\rm nl}=2\pi/\tau_{\rm nl}$. We focus on a spatial lag of $\ell=1$ $d_{\rm i}$, the ion-inertial length, a scale at which a majority of highly unstable modes are found.

 $PIC\ simulation$ — We analyze data obtained from a three-dimensional, fully kinetic, particle-in-cell (PIC) simulation [27]. The simulation has 2048^3 grid points, with $L=41.9\,d_{\rm i},\ \beta_{\rm p}=\beta_{\rm e}=0.5,\ m_{\rm p}/m_{\rm e}=50,\ \delta B/B_0=1.$ The analysis is performed on a snapshot late in time evolution of the simulation. For more details, refer to [27]. We emphasize that no attempt is made to closely align the simulation parameters with those of the magnetosheath or the solar wind.

Figure 1 shows the estimated values of probability density of $(\beta_{\parallel p}, R_p)$ -values in the 3D PIC data , along with the contours of constant instability growth rate, indicating involvement of $\beta_{\parallel p}$ -dependent constraints on R_p , in the simulation data. Although, for any given $\beta_{\parallel p}$ -value, a distribution of R_p -values is observed, the distribution's mode occurs near $R_p\approx 1$, and its width becomes progressively narrower with increased $\beta_{\parallel p}$. Thus, the plasma likely hosts processes that favor isotropic protontemperatures (limiting both $R_p>1$ and $R_p<1$) and

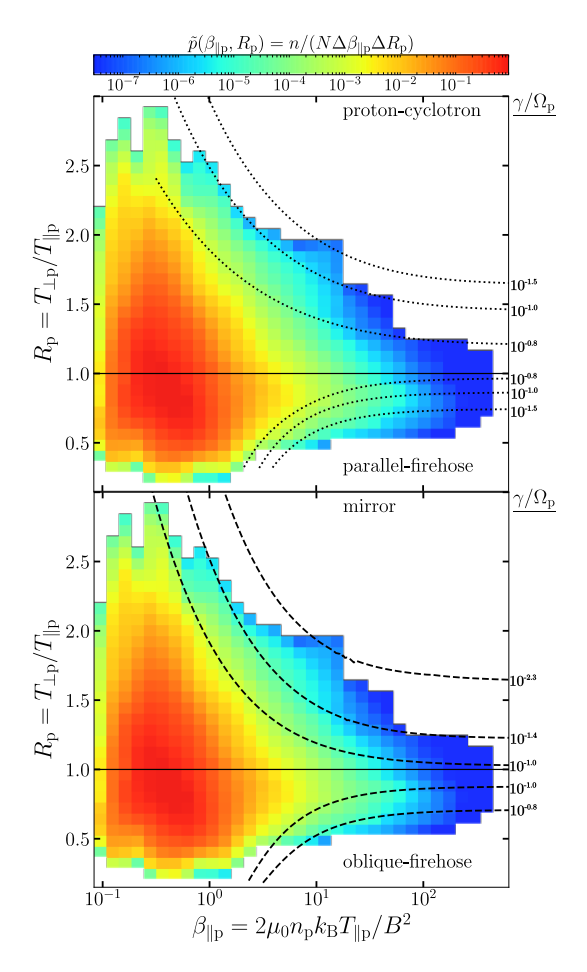


FIG. 1. Two plots of the estimated probability density, \tilde{p} , of $(\beta_{\parallel \mathrm{P}}, R_{\mathrm{P}})$ -values for the 3D PIC data. The two panels are identical except for the overlaid curves, which show contours of constant growth rate for different instabilities. The curves in the top panel show the parallel instabilities: the protoncyclotron $(R_{\mathrm{P}}>1)$ and parallel-firehose $(R_{\mathrm{P}}>1)$. The curves in the bottom panel show the oblique instabilities: the mirror $(R_{\mathrm{P}}>1)$ and oblique-firehose $(R_{\mathrm{P}}<1)$. Each contour is labeled with its growth rate, γ , in units of the proton cyclotron frequency, Ω_{P} .

these processes likely become more active at higher values of $\beta_{\parallel p}$. We believe these are the first reports of such $\beta_{\parallel p}$ -dependent constraints on R_p in a three-dimensional, fully kinetic PIC simulation. Similar plots are obtained for the solar wind [26] and magnetosheath [9].

The left panel of Fig. 2 shows the distribution of maximum growth rate, γ , (Eq. 4) for a plane perpendicular to the mean magnetic field, at $z \approx 35.6\,d_{\rm i}$. The center panel illustrates the nonlinear frequencies at each point, averaged over lags of $1\,d_{\rm i}$ along the x,y, and z directions. From the first two panels of Fig. 2, it is evident that both kinds of frequencies are distributed intermittently in space, with clusters of large values in similar regions. However, from the right panel, the ratio of these frequencies rarely exceeds unity. Even if both kind of processes

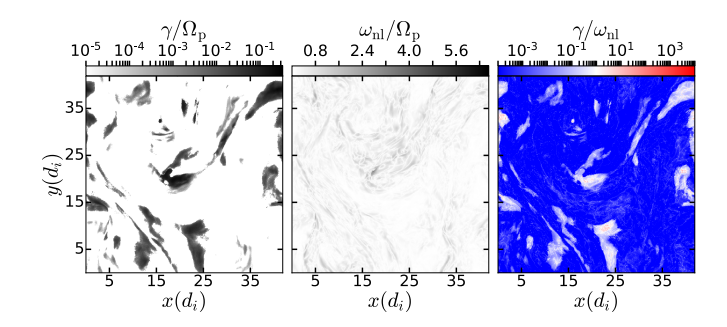


FIG. 2. Plots (from left to right) of maximum growth rate γ , nonlinear frequency $\omega_{\rm nl}$ at 1 $d_{\rm i}$, and the ratio $\gamma/\omega_{\rm nl}$ at $z\approx 35.6\,d_{\rm i}$ from PIC simulation.

are enhanced near the same regions of physical space, the non-linear processes are typically faster. Although Fig. 2 plots only one plane, later we show an analysis from the full 3D simulation domain.

In situ Observation— Though our analysis in the preceding section has important implications, the PIC simulation carries several limitations, e.g., artificial proton to electron mass ratio, small system size. Therefore, we next perform similar analyses, for two naturally occurring turbulent plasma systems: Earth's magnetosheath and the interplanetary solar wind.

We use burst-mode MMS [28] data sampled in the Earth's magnetosheath for several burst-mode periods in both quasi-parallel and quasi-perpendicular shocked plasmas, including the ones reported in [9]. MMS/Fast Plasma Investigation [29] moments provide $\beta_{\parallel p}$, R_p -values and magnetic-field measurements from the Flux Gate Magnetometer [30] are used to compute the longitudinal increment (Eq. 5) at a spatial separation of $1 d_i$. We select the magnetosheath intervals where the flow speed is greater than the Alfvén speed and use the Taylor hypothesis to convert the temporal separation to spatial separation $(\ell = -\langle |\mathbf{V}| \rangle \tau)$. The non-linear frequencies were computed from the magnetic-field increments and interpolated to the ion cadence of 150 ms. The instability growth rates are calculated at ion cadence from the $\beta_{\parallel p}$, R_p values.

The final statistics, shown later, are accumulated from all the intervals. However, in Fig. 3, we show, as an example, a 40 min burst-mode sample from 06:12:43 - 06:52:23 UTC on 26 December 2017. Note that this interval is typical and not chosen for any special properties, other that the preliminary observation that it is turbulent and contains current sheets [31, 32]. The bottom panel on the top plot of Fig. 3 clearly shows that the ratio $\gamma/\omega_{\rm nl}$ for this interval rarely exceeds unity.

In the bottom plot of Fig. 3, we show a similar analysis for 1 au solar wind. We use measurements from *Wind* satellite, accumulated over a period of about 10 years. We use 11 Hz magnetic field measurements from *Wind*'s

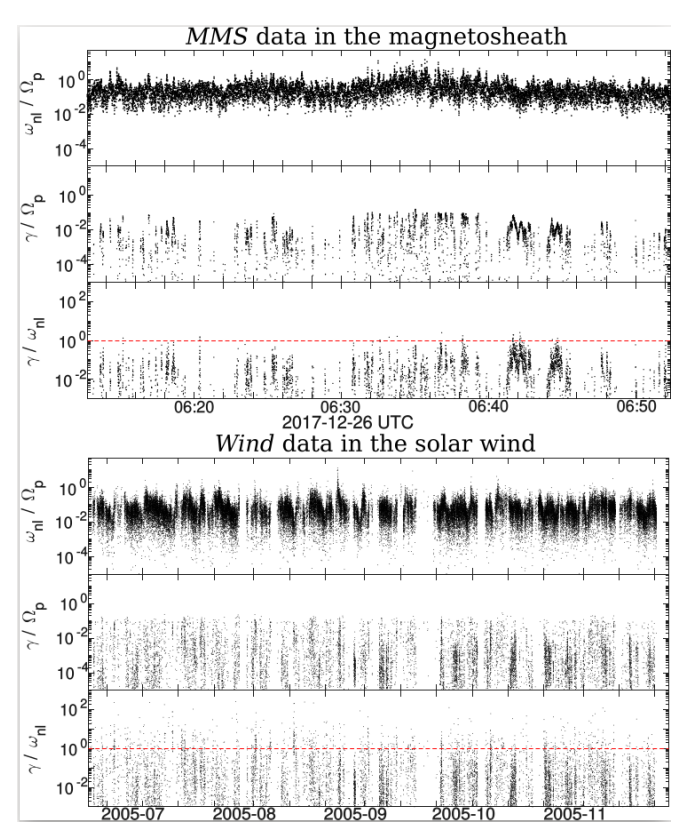


FIG. 3. Time series of the nonlinear frequency $\omega_{\rm nl}$ at $1\,d_{\rm i}$ (top), the maximum instability growth rates γ (middle), and the ratio $\gamma/\omega_{\rm nl}$ (bottom) for a burst-mode magnetosheath sample observed by the MMS spacecraft (top) and an interplanetary solar wind interval sampled by the Wind spacecraft (bottom). Note that due to the large difference in the measurement resolution of the MMS and Wind spacecraft, the time scales in the two figures are vastly different (~ 40 min versus ~ 4 months); however, they contain a similar number of correlation times of the respective data.

Magnetic Field Investigation [33] to calculate $\omega_{\rm nl}$ for a Taylor-shifted separation of $1\,d_{\rm i}$. The two Faraday cups in the Solar Wind Experiment [34] return one ion spectrum every $\approx 90\,{\rm s}$ and the $\omega_{\rm nl}$ values are interpolated to this cadence. A bi-Maxwellian distribution is fit to each ion spectrum to compute proton moments [35] and thus infer values of $R_{\rm p}$ and $\beta_{\parallel \rm p}$. The Wind data used here are identical to those reported in [26]. In the small sample of ≈ 4 months of Wind data, shown in the bottom plot of Fig. 3, the exhibited behavior closely resembles the magnetosheath results (Fig. 3, top), apart from the differences in time scales. Again, the nonlinear frequency, $\omega_{\rm nl}$, is greater than the instability growth rate, γ , for the majority, and the regions in which the growth rate is of relative significance are sporadic.

The main result of this paper is shown in Fig. 4. Here, we plot joint probability distribution functions of the instability growth rates (γ) and the non-linear frequencies

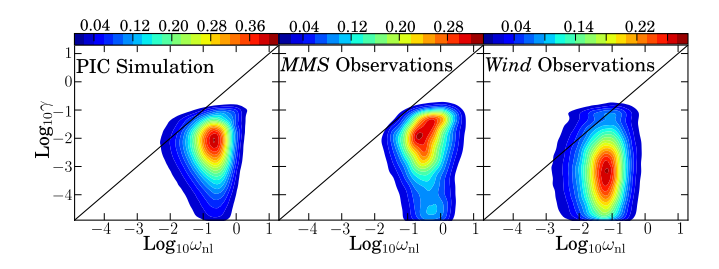


FIG. 4. Joint probability distribution functions of the maximum instability growth rate γ and the nonlinear frequency $\omega_{\rm nl}$ from PIC simulation, MMS data in the magnetosheath, and Wind data in the interplanetary solar wind.

 $(\omega_{\rm nl})$ for all three datasets. In all three cases, the core of the distribution resides well below the $\gamma=\omega_{\rm nl}$ line. From this result, we can conclude that for most data samples, the non-linear processes are faster than the linear-instability growth.

Discussion. Temperature-anisotropy driven microinstabilities are often considered to constrain the temperature anisotropy values in weakly-collisional plasmas [7, 36, 37]. Recall that the linear Vlasov theory of instabilities assumes a homogeneous background, in which background a small perturbation grows exponentially. The established success of linear-microinstability theories suggests that the conditions near the extremely anisotropic temperature may be uniform enough to justify an application of linear theories. Turbulence, on the other hand, is an intrinsically nonlinear process. Thin current sheets, and other coherent structures generated by the energy cascade, are sites of extreme temperature anisotropy [20] and therefore, the high growth rates due to the microinstabilities also reside in the same vicinity. It is therefore not a priori obvious whether the presence of intermittency and coherent structures favors or disfavors instabilities in comparison with nonlinear effects. This question has motivated the present study.

To address this question, we have examined the statistical distribution of growth rates associated with proton temperature-anisotropy driven microinstabilities and the local nonlinear time scales, in three distinct systems. The three systems cover different ranges of $(R_p, \beta_{\parallel p})$ -values among other parameters. However, both simulation and observation results show that, when the comparison is performed in this way, locally in space, a negligible fraction of the samples support long-lived linear instabilities. For the majority of cases, it appears that the nonlinear effects do not allow sufficient time for the instabilities to grow large enough to affect the global dynamics to any significant degree. In this regard it is interesting that the instabilities appear to delimit the anisotropies even though the theory assumes homogeneous perturbations. One possibility is if the initial fluctuations are large amplitude to begin with, in which case application

of a linear theory becomes questionable. In either case, clearly, a substantial revision in the present theoretical understanding is in order.

In this study, we have used a basic homogeneous plasma model to estimate the growth rate of pressure-driven instabilities. A more realistic extension will consider other ion species, as well as modifications to the linear theory introduced by the presence of strong spatial inhomogeneity near coherent structures. Finally, consideration of more general equilibrium VDFs may give rise to more rapid instability. Each of these refinements would represent a significant subsequent study.

TNP was supported by NSF SHINE Grant AGS-1460130 and NASA HGI Grant 80NSSC19K0284. WHM is a member of the MMS Theory and Modeling Team and was supported by NASA Grant NNX14AC39G. The research of SPG was supported by NASA grant NNX17AH87G.

This study used Level 2 FPI and FIELDS data according to the guidelines set forth by the *MMS* instrumentation team. All data are freely available at https://lasp.colorado.edu/MMS/sdc/. We thank the *MMS* SDC, FPI, and FIELDS teams for their assistance with this study.

Wind SWE and MFI data are available from CDAWeb (https://cdaweb.gsfc.nasa.gov/). The authors thank the Wind team for the Wind magnetic field and plasma data.

The bi-Maxwellian analysis code is summarized in [35].

The simulation described in this paper was performed as a part of the Blue Waters sustained-petascale computing project, which was supported by the National Science Foundation (awards OCI-0725070 and ACI-1238993) and the State of Illinois. Blue Waters allocation was provided by NSF PRAC award 1614664.

The authors would like to thank Rohit Chhiber for useful discussions and Yan Yang for helping to prepare the PIC dataset.

SUPPLEMENTAL MATERIAL

The first three panels of Fig. 5 show the three parameters — R_p , $\beta_{\parallel p}$, and J_z — across a plane at $z\approx 35.6\,d_{\rm i}$ of the simulation box. The system is strongly turbulent and exhibits structures of various scales. The extreme values of each parameter occur in distinct regions that occupy only small fractions of the total volume. That is, these quantities are intermittent, which is correlated with the existence of sharp gradients and coherent structures. Further, the extreme values of R_p and $\beta_{\parallel p}$ reside near (but not necessarily exactly coincident with) the extreme values of J_z . These concentrations of current densities frequently correspond to current sheets.

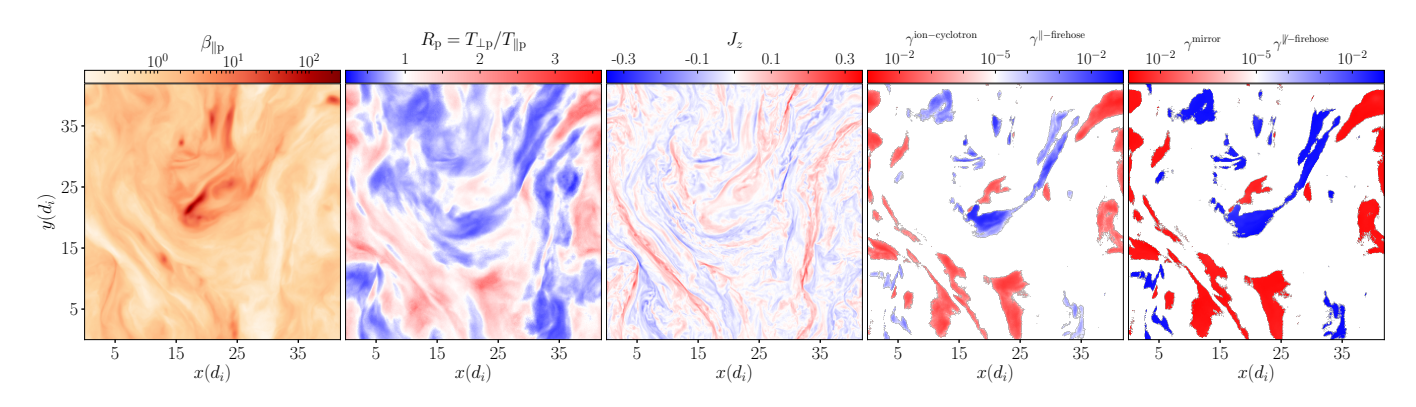


FIG. 5. Colorplot of (left to right) $\beta_{\parallel p}$, R_p and J_z , from a fully kinetic 3D PIC simulation at $z \approx 35.6 \, d_i$. The fourth and fifth panels show the spatial distribution of growth rate in units of proton-cyclotron frequency, γ/Ω_p , for parallel and oblique propagation corresponding to the first two panels.

Using the method described in the main text, we compute γ for the $(\beta_{\parallel p}, R_p)$ -pair at each grid point of the simulation, where γ is the maximum value of growth rate for all possible values of propagation vector (k), for a given instability. The fourth panel of Fig. 5 shows the spatial distribution of growth rates for the solutions with positive growth rates, corresponding to the first two panels of the same figure. As described in main article, for $\gamma_{\rm max}$, we imposed a cut-off at $10^{-5}\Omega_{\rm p}$; thus growth rates less than $10^{-5}\Omega_{\rm p}$ are considered to be 0. The fourth panel of Fig. 5 corresponds to the parallel modes (cyclotron for $R_{\rm p} > 1$ and parallel firehose for $R_{\rm p} < 1$), whereas the fifth panel is for the oblique propagation (mirror for $R_p > 1$ and oblique firehose for $R_p < 1$). The nearly equal abundance of blue and red color in the fifth panel implies that the $\beta_{\parallel p}$ and R_p or both have high and low enough values to excite all the modes fairly well.

Comparing the second panel to the fourth and fifth of Fig. 5, we see that values of $\gamma > 0$ are concentrated in distinct, filament-like regions of the xy-plane where extreme values of temperature anisotropy also occur.

- R. Bruno and V. Carbone, Living Reviews in Solar Physics 2, 4 (2005).
- [2] G. Zimbardo, A. Greco, L. Sorriso-Valvo, S. Perri, Z. Vörös, G. Aburjania, K. Chargazia, and O. Alexandrova, Space Science Reviews 156, 89 (2010).
- [3] W. G. Pilipp, H. Miggenrieder, M. D. Montgomery, K.-H. Mühlhäuser, H. Rosenbauer, and R. Schwenn, Journal of Geophysical Research: Space Physics 92, 1075 (1987).
- [4] M. Maksimovic, I. Zouganelis, J.-Y. Chaufray, K. Issautier, E. E. Scime, J. E. Littleton, E. Marsch, D. J. McComas, C. Salem, R. P. Lin, and H. Elliott, Journal of Geophysical Research: Space Physics 110, A09104 (2005).
- [5] E. Marsch, Living Reviews in Solar Physics 3, 1 (2006).
- [6] S. P. Gary, R. M. Skoug, J. T. Steinberg, and C. W.

- Smith, Geophysical Research Letters 28, 2759 (2001).
- [7] J. C. Kasper, A. J. Lazarus, and S. P. Gary, Geophysical Research Letters 29, 20 (2002).
- [8] P. Hellinger, P. Trávníček, J. C. Kasper, and A. J. Lazarus, Geophysical Research Letters 33, L09101 (2006), 10.1029/2006GL025925.
- [9] B. A. Maruca, A. Chasapis, S. P. Gary, R. Bandyopadhyay, R. Chhiber, T. N. Parashar, W. H. Matthaeus, M. A. Shay, J. L. Burch, T. E. Moore, C. J. Pollock, B. J. Giles, W. R. Paterson, J. Dorelli, D. J. Gershman, R. B. Torbert, C. T. Russell, and R. J. Strangeway, The Astrophysical Journal 866, 25 (2018).
- [10] S. P. Gary, Theory of Space Plasma Microinstabilities (Cambridge University Press, Cambridge, UK, 1993).
- [11] S. D. Bale, P. J. Kellogg, F. S. Mozer, T. S. Horbury, and H. Reme, Phys. Rev. Lett. 94, 215002 (2005).
- [12] A. Greco, F. Valentini, S. Servidio, and W. H. Matthaeus, Phys. Rev. E 86, 066405 (2012), 10.1103/PhysRevE.86.066405.
- [13] S. Servidio, F. Valentini, D. Perrone, A. Greco, F. Califano, W. H. Matthaeus, P. Veltri, and Veltri, Journal of Plasma Physics 81, 3207 (2015).
- [14] M. W. Kunz, A. A. Schekochihin, and J. M. Stone, Phys. Rev. Lett. 112, 205003 (2014).
- [15] S. A. Markovskii, B. J. Vasquez, and B. D. G. Chandran, The Astrophysical Journal 875, 125 (2019).
- [16] P. Hellinger, L. Matteini, S. Landi, L. Franci, A. Verdini, and E. Papini, "Turbulence vs. fire hose instabilities: 3-d hybrid expanding box simulations," (2019), arXiv:1908.07760 [physics.space-ph].
- [17] K. T. Osman, W. H. Matthaeus, B. Hnat, and S. C. Chapman, Phys. Rev. Lett. 108, 261103 (2012).
- [18] S. Servidio, K. T. Osman, F. Valentini, D. Perrone, F. Califano, S. Chapman, W. H. Matthaeus, and P. Veltri, The Astrophysical Journal 781, L27 (2014).
- [19] H. Karimabadi, V. Roytershteyn, M. Wan, W. H. Matthaeus, W. Daughton, P. Wu, M. Shay, B. Loring, J. Borovsky, E. Leonardis, S. C. Chapman, and T. K. M. Nakamura, Physics of Plasmas 20, 012303 (2013).
- [20] A. Greco, F. Valentini, S. Servidio, and W. H. Matthaeus, Phys. Rev. E 86, 066405 (2012).
- [21] T. N. Parashar and W. H. Matthaeus, Astrophys. J. 832, 57 (2016), arXiv:1610.02912 [physics.space-ph].

- [22] W. H. Matthaeus, S. Oughton, K. T. Osman, S. Servidio, M. Wan, S. P. Gary, M. A. Shay, F. Valentini, V. Roytershteyn, H. Karimabadi, and S. C. Chapman, Astrophys. J. 790, 155 (2014).
- [23] K. G. Klein, B. L. Alterman, M. L. Stevens, D. Vech, and J. C. Kasper, Phys. Rev. Lett. 120, 205102 (2018).
- [24] W. H. Matthaeus, M. Wan, S. Servidio, A. Greco, K. T. Osman, S. Oughton, and P. Dmitruk, Philosophical Transactions of the Royal Society of London A: Mathematical, Physical and Engineering Sciences 373 (2015), 10.1098/rsta.2014.0154.
- [25] M. Wan, W. H. Matthaeus, V. Roytershteyn, T. N. Parashar, P. Wu, and H. Karimabadi, Physics of Plasmas 23, 042307 (2016).
- [26] B. A. Maruca, J. C. Kasper, and S. P. Gary, The Astrophysical Journal 748, 137 (2012).
- [27] V. Roytershteyn, H. Karimabadi, and A. Roberts, Philosophical Transactions of the Royal Society A: Mathematical, Physical and Engineering Sciences 373, 20140151 (2015).
- [28] J. L. Burch, T. E. Moore, R. B. Torbert, and B. L. Giles, Space Science Reviews 199, 5 (2016).
- [29] C. Pollock, T. Moore, A. Jacques, J. Burch, U. Gliese, Y. Saito, T. Omoto, L. Avanov, A. Barrie, V. Coffey, J. Dorelli, D. Gershman, B. Giles, T. Rosnack, C. Salo, S. Yokota, M. Adrian, C. Aoustin, C. Auletti, S. Aung, V. Bigio, N. Cao, M. Chandler, D. Chornay, K. Christian, G. Clark, G. Collinson, T. Corris, A. DeLosSantos, R. Devlin, T. Diaz, T. Dickerson, C. Dickson, A. Diekmann, F. Diggs, C. Duncan, A. Figueroa-Vinas, C. Firman, M. Freeman, N. Galassi, K. Garcia, G. Goodhart, D. Guererro, J. Hageman, J. Hanley, E. Hemminger, M. Holland, M. Hutchins, T. James, W. Jones, S. Kreisler, J. Kujawski, V. Lavu, J. Lobell, E. LeCompte, A. Lukemire, E. MacDonald, A. Mariano, T. Mukai, K. Narayanan, Q. Nguyan, M. Onizuka, W. Paterson, S. Persyn, B. Piepgrass, F. Cheney, A. Rager, T. Raghuram, A. Ramil, L. Reichen-

- thal, H. Rodriguez, J. Rouzaud, A. Rucker, Y. Saito, M. Samara, J.-A. Sauvaud, D. Schuster, M. Shappirio, K. Shelton, D. Sher, D. Smith, K. Smith, S. Smith, D. Steinfeld, R. Szymkiewicz, K. Tanimoto, J. Taylor, C. Tucker, K. Tull, A. Uhl, J. Vloet, P. Walpole, S. Weidner, D. White, G. Winkert, P.-S. Yeh, and M. Zeuch, Space Science Reviews 199, 331 (2016).
- [30] C. T. Russell, B. J. Anderson, W. Baumjohann, K. R. Bromund, D. Dearborn, D. Fischer, G. Le, H. K. Leinweber, D. Leneman, W. Magnes, J. D. Means, M. B. Moldwin, R. Nakamura, D. Pierce, F. Plaschke, K. M. Rowe, J. A. Slavin, R. J. Strangeway, R. Torbert, C. Hagen, I. Jernej, A. Valavanoglou, and I. Richter, Space Science Reviews 199, 189 (2016).
- [31] T. N. Parashar, A. Chasapis, R. Bandyopadhyay, R. Chhiber, W. H. Matthaeus, B. Maruca, M. A. Shay, J. L. Burch, T. E. Moore, B. L. Giles, D. J. Gershman, C. J. Pollock, R. B. Torbert, C. T. Russell, R. J. Strangeway, and V. Roytershteyn, Phys. Rev. Lett. 121, 265101 (2018).
- [32] R. Qudsi and . et al., In Preparation (2020).
- [33] R. P. Lepping, M. H. Acũna, L. F. Burlaga, W. M. Farrell, J. A. Slavin, K. H. Schatten, F. Mariani, N. F. Ness, F. M. Neubauer, Y. C. Whang, J. B. Byrnes, R. S. Kennon, P. V. Panetta, J. Scheifele, and E. M. Worley, Space Science Reviews 71, 207 (1995).
- [34] K. W. Ogilvie, D. J. Chornay, R. J. Fritzenreiter, F. Hunsaker, J. Keller, J. Lobell, G. Miller, J. D. Scudder, E. C. Sittler, R. B. Torbert, D. Bodet, G. Needell, A. J. Lazarus, J. T. Steinberg, J. H. Tappan, A. Mavretic, and E. Gergin, Space Science Reviews 71, 55 (1995).
- [35] B. A. Maruca and J. C. Kasper, **52**, 723 (2013).
- [36] P. Hellinger, P. Trávníček, J. C. Kasper, and A. J. Lazarus, Geophysical Research Letters 33, L09101 (2006).
- [37] D. Verscharen, K. G. Klein, and B. A. Maruca, Living Reviews in Solar Physics 16, 5 (2019).